HOLOGRAPHICALLY-INDUCED SAWS AT A SOLID- OR LIQUID-SOLID INTERFACE

S. M. Gracewski

Mechanical Engineering
University of Rochester
Rochester, NY 14627

R. J. Dwayne Miller

Department of Chemistry
University of Rochester
Rochester, New York 14627

INTRODUCTION

Lasers offer a non-contact method for generating ultrasound. The main advantages are that specimen can be scanned more easily and the complications of a coupling layer or liquid are eliminated. Also, more accurate velocity measurements can be obtained using lasers and for holographic generation, higher frequency coherent waves can be obtained. Lasers have been used to generate ultrasonic waves in many configurations, including the generation of bulk longitudinal and shear waves, Rayleigh waves along solid surfaces, and Lamb modes in solid layers. General reviews of laser generation techniques can be found in [1] and [2].

Excitation of surface waves along a solid boundary by transient laser heating was first demonstrated by Lee and White [3]. In the simplest configuration, a point source of light is directed at a solid boundary. Line [4] and ring [5] sources have been used to modify the directivity pattern of the resulting surface acoustic waves (SAWs) and increase the acoustic energy at the location of interest. To generate surface waves of predominately one frequency (or wavelength), masks [6] have been used to produce a periodic heating pattern. Alternatively, coherent waves can be generated by the harmonic interference pattern of two crossed laser pulses [7–8].

The analysis presented here models the holographic wave generation by thermal surface heating due to a pulsed laser interference pattern. The exact elastic wave solution accounting for the finite depth of heating in the substrate will be presented here, rather than using an approximate boundary condition to model the applied field as is typically found in the literature. The resulting SAW wavelength Λ will be equal to the interference pattern spacing

$$\Lambda = \frac{\lambda_o}{2 \sin\left(\frac{\theta}{2}\right)},$$

where λ_o is the wavelength of the laser light and θ is the angle between the two incident laser pulses (Fig. 1). The SAW amplitude can be determined by diffraction of a third time-delayed laser pulse of lower intensity. In this situation, only the standing wave pattern within the area illuminated by the generation laser is of interest. From measurements of diffraction efficiency as a function of the time delay of the detection pulse, the SAW amplitude, wavespeed, and attenuation can be determined. The main advantage of this laser interference technique is that coherent, high-frequency (up to ~100GHz) waves can be generated. In addition, the SAW wave frequency is continuously tunable by adjusting the angle θ between the two generation laser pulses.

Review of Progress in Quantitative Nondestructive Evaluation, Vol. 9
Edited by D.O. Thompson and D.E. Chimenti
Plenum Press, New York, 1990

The structure considered here consists of a thin solid layer perfectly bonded to a solid substrate and in contact above with a liquid (liquid–solid–solid structure), as shown in Fig. 1. The solid substrate and liquid extend far enough away from the layer interface such that reflections from their outer boundaries can be neglected and therefore these boundaries can be modeled as being at infinity. The solid layer and liquid are assumed to be transparent. Therefore the two generation laser pulses cross along the interface between the layer and substrate and are 'absorbed by the substrate generating a heating pattern that is harmonic along the boundary and decaying exponentially with depth into the solid. In addition, heating of the solid layer and liquid by diffusion will be approximated by a temperature pattern which is again harmonic along the boundary and decays exponentially into the liquid. The solid layer will be assumed thin so that the temperature can be modeled as constant across the layer. Since only the standing-wave pattern, well within the spot illuminated by the generation lasers, is of interest, edge effects of the illuminated area can be neglected and the heating pattern as well as the elastic response can be modeled as harmonic parallel to the interface for all x_1. This approximation is valid if the interference pattern spacing is much smaller than the laser spot size.

In this paper, the solution process will be summarized and the solution will be stated for the limiting case of the layer thickness equal to zero (i.e., for the liquid–solid structure). Numerical results will be presented for materials of interest along with corresponding experimental results. Also, the effects of a thin layer on the surface displacements will be examined.

PROBLEM STATEMENT

The plane-strain solution will be derived assuming the substrate and the solid layer bonded to it are isotropic and linearly elastic and the liquid is isotropic and inviscid. The density and longitudinal and shear wavespeeds will be denoted by ρ, c_d, and c_t, respectively. Layer quantities will be distinguished with the use of a prime and liquid quantities with a subscript or superscript L

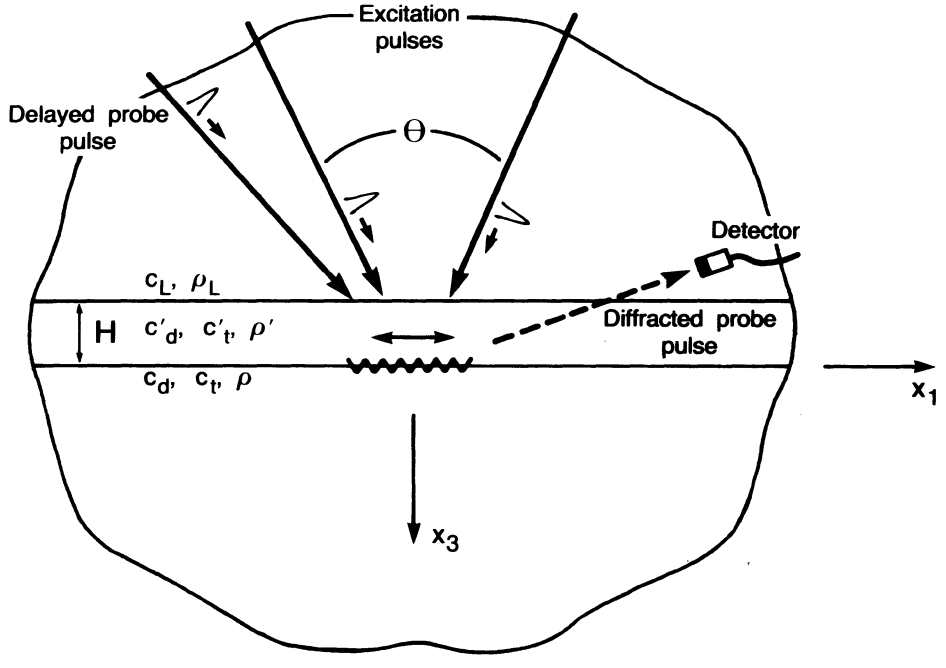

Fig. 1 Liquid-solid-solid structure showing the optical generation and detection pulse configuration.

(The longitudinal wavespeed in the liquid will be denoted by c_L.). In terms of the Lame constants λ and μ, the wavespeeds can be written as $c_d = \sqrt{\lambda + 2\mu/\rho}$ *and* $c_t = \sqrt{\mu/\rho}$. The vector equation of motion in terms of the displacement $\mathbf{u}$ is

$$(\lambda + 2\mu)\nabla\nabla \cdot \mathbf{u} + \mu\nabla^2\mathbf{u} - \rho\ddot{\mathbf{u}} = \overline{\alpha}(3\lambda + 2\mu)\nabla(T - T_o) \ , \tag{1}$$

where $\overline{\alpha}$ is the linear thermal expansion coefficient and

$$\nabla = \frac{\partial}{\partial x_1}\mathbf{e}_1 + \frac{\partial}{\partial x_3}\mathbf{e}_3 \ .$$

Equation (1) must be satisfied in each media subject to the applied temperature fields

$$(T - T_o) = \frac{\Delta T_{max}}{2}\left[1 + \sin\left(\frac{2\pi x_1}{\Lambda}\right)\right] e^{-\alpha x_3} U(t) \ , \tag{2a}$$

in the substrate,

$$(T - T_o)' = \frac{\Delta T_{max}}{2}\left[1 + \sin\left(\frac{2\pi x_1}{\Lambda}\right)\right] U(t) \ , \tag{2b}$$

in the layer, and

$$(T - T_o)^L = \frac{\Delta T_{max}}{2}\left[1 + \sin\left(\frac{2\pi x_1}{\Lambda}\right)\right] e^{\beta(x_3 + H)} U(t) \ , \tag{2c}$$

in the liquid, where U(t) is the unit step function, T_o is the initial temperature, and the coordinate system is as shown in Fig. 1. For the temperature fields to have a step function time dependence, the excitation laser pulse length and the molecular relaxation times must be much shorter than the acoustic time constant such that the heat deposition can be considered instantaneous. Also, diffusion is neglected during the experimental time scale, except to approximate initial heating of the layer and liquid. The equations of motion (Eqn. (1)), must be solved for the applied temperature fields given in Eqn. (2) subject to zero initial conditions $\mathbf{u} = \dot{\mathbf{u}} = \mathbf{0}$, and the radiation conditions and the boundary conditions

$$\begin{aligned} \mathbf{u} &= \mathbf{u}' \ , \\ \tau \cdot \mathbf{e}_3 &= \tau' \cdot \mathbf{e}_3 \ , \end{aligned} \tag{3a}$$

at $x_3 = 0$, and

$$\begin{aligned} \mathbf{u}' &= \mathbf{u}^L \ , \\ \tau' \cdot \mathbf{e}_3 &= \mathbf{0} \ , \end{aligned} \tag{3b}$$

at $x_3 = -H$, where τ is the stress tensor.

SPATIALLY HARMONIC SOLUTION

The analytic solution and numerical results will be presented for the spatially harmonic terms in the applied temperature field since only the spatially harmonic response can be measured experimentally by detecting the intensity of the diffracted third time-delayed laser pulse. Results for rutile (TiO_2) in contact with water and with ethanol will be compared with experimental results. The spatially constant terms in the applied temperature fields will produce longitudinal waves only, propagating normal to the material interfaces. The solution procedure will be summarized here and the result for the liquid–solid structure will be given. For more detail and the result for the liquid–solid–solid structure, consult reference [9].

The solution for the complete liquid–solid–solid structure was obtained in terms of the wave potentials, by first assuming an appropriate form for the solution which is harmonic in the x_1 direction and taking a Laplace Transform in time to reduce the equations to ordinary differential equations. The solution to the ordinary differential equations was obtained and substituted into the boundary conditions to determine the constants of integration. The resulting 7x7 matrix equation

was solved symbolically using MACSYMA [10]. The final result, obtained by taking an inverse Laplace Transform is in the form of infinite integrals in the Laplace Transform variable. The resulting solution for the displacements in the solid for the liquid–solid structure is

$$u_1 = \frac{\cos(k_o x_1)}{2\pi i} \lim_{\gamma\to\infty} \int_{\zeta-i\gamma}^{\zeta+i\gamma} \left[k_o \left(D_6 e^{-b_d x_3} + M e^{-\alpha x_3}\right) + b_t D_7 e^{-b_t x_3}\right] e^{\omega t}\, d\omega \,,$$

$$u_3 = -\frac{\sin(k_o x_1)}{2\pi i} \lim_{\gamma\to\infty} \int_{\zeta-i\gamma}^{\zeta+i\gamma} \left[b_d D_6 e^{-b_d x_3} + \alpha M e^{-\alpha x_3} + k_o D_7 e^{-b_t x_3}\right] e^{\omega t}\, d\omega \,, \tag{4}$$

where

$$D_6 = \frac{N_{6a}}{\Delta} M + \frac{N_{6c}}{\Delta} M_L \,,$$
$$D_7 = \frac{N_{7a}}{\Delta} M + \frac{N_{7c}}{\Delta} M_L \,,$$

and

$$N_{6a} = -\rho b_L \left(z^2 - 4\alpha b_t k_o^2\right) + \rho_L \alpha k_t^4 \,,$$
$$N_{6c} = \rho_L (b_L - \beta) k_t^2 z \,,$$
$$N_{7a} = 2\rho (b_d - \alpha) k_o b_L z \,,$$
$$N_{7c} = -2\rho_L (b_L - \beta) k_o b_d k_t^2 \,,$$
$$\Delta = \rho b_L \left(z^2 - 4 b_d b_t k_o^2\right) + \rho_L b_d \,,$$

$$M = \frac{\overline{\alpha}(3\lambda + 2\mu)}{(\lambda + 2\mu)(\alpha^2 - b_d^2)\omega} \frac{\Delta T_{max}}{2} \,,$$
$$M_L = \frac{3\overline{\alpha_L}}{(\beta^2 - b_L^2)\omega} \frac{\Delta T_{max}}{2} \,,$$

and with $k_o = 2\pi/\Lambda$, $b_d = \sqrt{k_o^2 + \omega^2/c_d^2}$, $b_t = \sqrt{k_o^2 + \omega^2/c_t^2}$, $b_L = \sqrt{k_o^2 + \omega^2/c_L^2}$, and $z = 2k_o^2 + k_t^2$. Equations (4) must be integrated numerically, along a contour that avoids the zeros of Δ and the branch cuts of the square-root functions b_d, b_t, and b_L, which are determined by the radiation condition.

RESULTS

Numerical results are presented in nondimensional terms for normal and transverse displacements versus time for material parameters that correspond to experiments. Graphs of measured diffracted pulse intensity versus time are first given in Fig. 2a for an n-TiO_2 crystal in air and in Fig. 2b for an n-TiO_2 crystal in water and in ethanol. The signal due to the elastic response is superimposed on an initially large, but rapidly decaying signal resulting from the diffraction grating generated by free carriers. (See ref. [8] for a discussion of the free carrier diffraction grating and experimental details.) In Fig. 2a, the elastic response consists of a single frequency, which corresponds to the Rayleigh wavespeed for TiO_2. In Fig. 2b, for both n-TiO_2 in water and in ethanol, there is an oscillation of a lower frequency superimposed on the Rayleigh mode oscillation. This lower-frequency component corresponds to the Stoneley mode with energy predominantly in the liquid. There also appears to be a third component in the TiO_2 – water result which has a frequency close to the Rayleigh wave mode and dies away within a few cycles.

The numerical results were calculated for a solid substrate with c_d=7900m/s, c_t=5400m/s, ρ=4.26x10^{3}kg/m^3, $\overline{\alpha}$=9.943x10^{-6}/°C, α=1/700x10^{-10}/m, and Λ=2.6x10^{-6}m. These wavespeeds are correct for the (001) plane of TiO_2 and $\overline{\alpha}$ was set equal to the coefficient of linear expansion normal to this plane. The results are presented in nondimensional form with nondimensional

displacements $\hat{u}_i = k_o u_i$ and nondimensional time $\hat{t} = tc_R/\Lambda$, where c_R=4783m/s is the Rayleigh wavespeed calculated from the values of c_d and c_t. The solid curve in Fig. 3a. shows the normal surface displacement at $\hat{x}_1 = \pi/2$ for a solid-vacuum structure. The initial rapid rise is followed by a nearly harmonic oscillation at the Rayleigh wave frequency. This result agrees with the measured result in Fig. 2a. The calculated result for a solid-water interface with heating only in the solid is shown as the dashed curve in Fig. 3a. The material parameters for water used in the calculation are c_L=1490m/s, ρ_L=1.0x10^{3}kg/m^3, and$\overline{\alpha_L}$=70x10^{-6}/°C. The addition of the liquid causes the peak-to-peak amplitude of the Rayleigh wave to decay with time. This is consistent with the well known fact that energy leaks into the liquid when a ('Leaky') Rayleigh wave is propagated along a solid-liquid interface. There is no evidence of the Stoneley mode, which propagates with a wavespeed approximately equal to the longitudinal wavespeed of the liquid with most of its energy in the liquid, indicating that heating of the liquid must occur in order to excite this wave. The transverse surface displacement at $\hat{x}_1 = 0$ is plotted in Fig. 3b. for the solid-vacuum and solid-water structures with heating of the solid only. The presence of a surface-skimming longitudinal wave in the solid is believed to cause the initial non-periodic displacements. This contribution dies out rapidly for the solid-vacuum boundary, but continues across the entire plot for the solid-liquid interface.

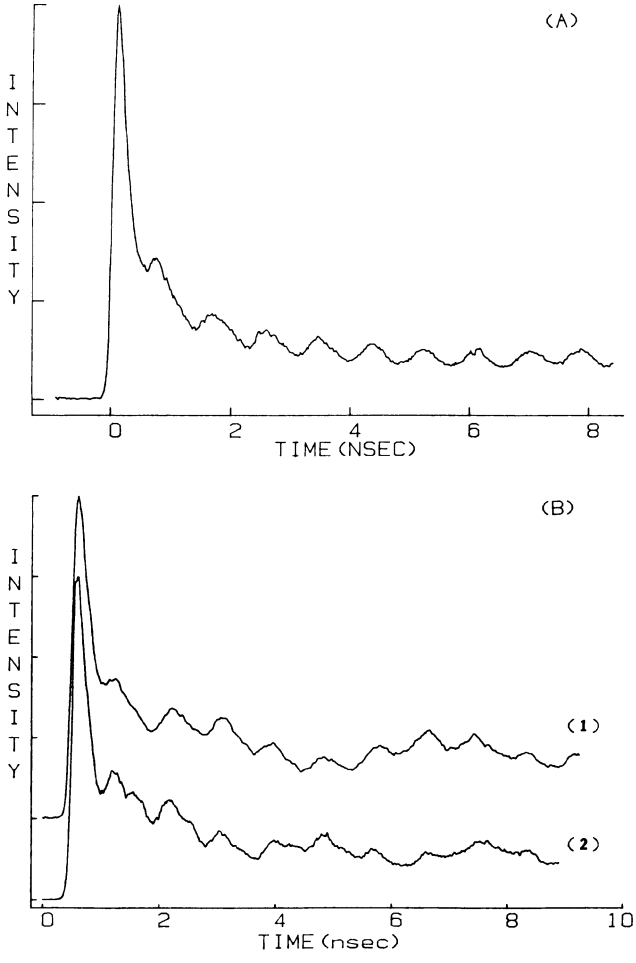

Fig. 2 Measured diffracted pulse intensity versus time showing elastic wave response for an n-TiO_2 surface (doping concentration = 4x10^{18}/cc) (a) in air, (b1) in neat ethanol, and (b2) in 1M Na_2SO_4 and 0.054M NaOH in H_2O.

Figs. 4a and 4b show the results for solid-vacuum, solid-water, solid-ethanol interfaces. The material parameters for ethanol used in the calculations are c_L=1200m/s, ρ_L=0.791x10^{3}kg/m^3, and$\overline{\alpha_L}$=350x10^{-6}/°C. For both liquids, the value for the decay constant β=1/300x10^{-10} was used based on the heat diffusion into the liquid within one acoustic cycle. This represents a maximum value, since heat must be deposited within $\sim 1/6$ acoustic cycle for coherent generation. These curves are calculated for constant average heat input per unit surface area Q=5x10^{4}J/cm^2 and therefore the amplitude of the Rayleigh wave is lower in the solid-liquid structures since less energy is deposited into the solid. For both liquids, the normal displacement plotted in Fig. 4a consists of the oscillation due to the Stoneley mode superimposed on the Rayleigh mode oscillation, as in the experimental results shown in Fig. 2b. Also, there is a slight phase shift in the Rayleigh mode oscillation for both liquids. In the corresponding transverse displacements in Fig. 3b., the contribution from the solid longitudinal grazing wave component last a longer time than for the solid-vacuum structure.

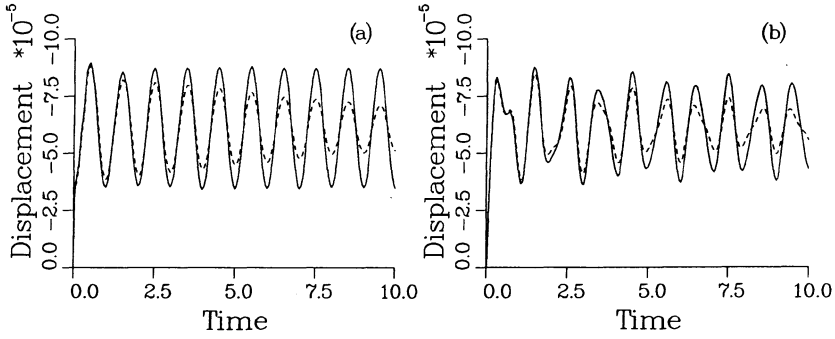

Fig. 3 Nondimensional surface displacements versus nondimensional time for a model of n-TiO_2 in a vacuum (solid line) and n-TiO_2 in water (dashed line), with heating of the solid only: (a) Normal displacement at $\hat{x}_1 = \pi/2$ and (b) Transverse displacement at $\hat{x}_1 = 0$.

The solid curves in Fig. 5 are identical to the dashed curves in Fig. 4 for the solid-water interface. The dashed curve in Fig. 5 shows the effect of the addition of a a solid layer with c_d=4100m/s, c_t=1900m/s, ρ=0.92kg/m^3, $\overline{\alpha_L}$=70x10^{-6}/°C, and H=200x10^{-10}m. These values were chosen to approximate the material characteristics of an 'ice' layer which models the postulated restructuring of a layer of water near the solid interface. It was proposed that a plate mode within this layer could be the source of the experimentally-observed third mode. The numerical results show that the 'ice' layer decreases the Rayleigh wave amplitude slightly, but an additional mode is not evident in the plot of the normal surface displacements. This result suggests that there is another cause for the third mode in the experimental results for the solid-water interface. The bulk wave contribution which decays with time and makes a larger contribution for the liquid-solid structure than for the vacuum-solid structure, as evident in the transverse displacement plots, may be the cause of this third component.

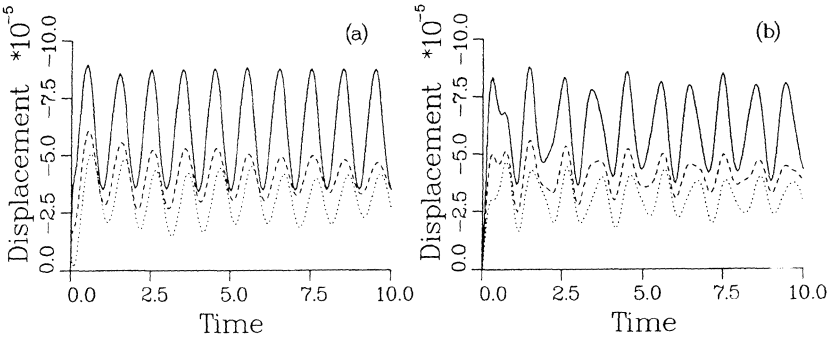

Fig. 4 Nondimensional surface displacements versus nondimensional time for a model of n-TiO_2 in vacuum (solid line) , in water (dashed line) and n-TiO_2 in ethanol (dotted line), with heating of the liquid estimated by diffusion: (a) Normal displacement at $\hat{x}_1 = \pi/2$ and (b) Transverse displacement at $\hat{x}_1 = 0$.

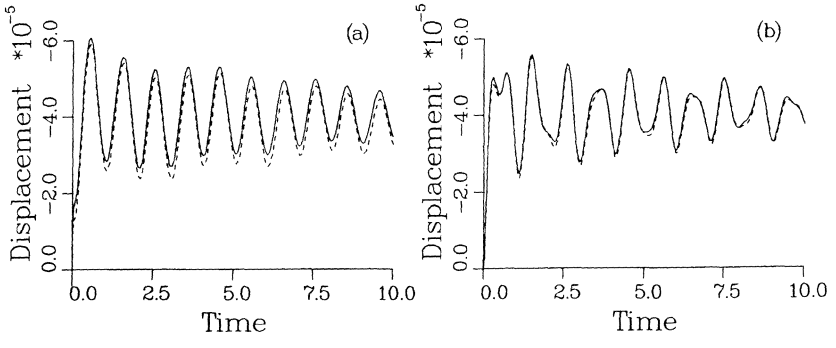

Fig. 5 Nondimensional displacements at the substrate boundary versus nondimensional time for a model of n-TiO_2 in water without (solid line) and with a solid 'ice' layer (dashed line), with heating of the all three materials: (a) Normal displacement at $\hat{x}_1 = \pi/2$ and (b) Transverse displacement at $\hat{x}_1 = 0$.

ACKNOWLEDGEMENT

This work was supported by the National Science Foundation under Grant No. ECS-860596.

REFERENCES

1. D. A. Hutchins, in Physical Acoustics, edited by W. P. Mason and R. N. Thurston (Academic Press, New York, 1988), vol. XVIII, Chap. 2.
2. G. Birnbaum and G. S. White, in Nondestructive Testing, edited by R. S. Sharpe (Academic Press, London, 1984), Vol. 7, Chap. 8.
3. R. E. Lee and R. M. White, Appl. Phys. Lett., 12(1),12 (1968).
4. A. M. Aindow, R. J. Dewhurst, and S. B. Palmer, Opt. Comm., 42,116 (1982).
5. P. Cielo, F. Nadeau, and M. Lamontagne, Ultrasonics, 23, 55 (1985).
6. E. A. Ash, I Dieulesaint, and H. Rakouth, Electronic Lett., 16(12), 470 (1980).
7. G. Cachier, Appl. Phys. Lett., 17,10,419 (1970).
8. J. J. Kasinski, L. Gomez-Jahn, S. M. Gracewski, and R. J. D. Miller, J. Chem. Phys., 90(2), 1253 (1989).
9. S. M. Gracewski and R. J. D. Miller, submitted to J. Acoust. Soc. Am., (1989).
10. MACSYMA Reference Manual, The Math Lab Group, Laboratory for Computer Science, Massachusetts Institute of Technology, (1983).